Image Denoising Using a New Implementation of the Hyperanalytic Wavelet Transform

Ioana Firoiu, Corina Nafornita, *Member, IEEE*,
Jean-Marc Boucher, *Senior Member, IEEE*, and Alexandru Isar, *Member, IEEE*

***Abstract*—Shift invariance associated with good directional selectivity is important for the use of a wavelet transform (WT) in many fields of image processing. Generally, complex wavelet transforms, e.g., the double-tree complex WT (DTCWT), have these useful properties. In this paper, we propose the use of a recently introduced implementation of such a WT, namely, the hyperanalytic WT (HWT), in association with filtering techniques already used with the discrete WT (DWT). The result is a very simple and fast image denoising algorithm. Some simulation results and comparisons prove the performance obtained using the new method.**

***Index Terms*—Directional selectivity, hyperanalytic wavelet transform (HWT), image denoising, maximum *a posteriori* (MAP) filter.**

I. Introduction

THROUGHOUT recent years, many wavelet transforms (WTs) have been used to operate denoising. The first one was the discrete WT (DWT) [1]. It has three main disadvantages [2]: lack of shift invariance, lack of symmetry of the mother wavelets, and poor directional selectivity. These disadvantages can be diminished using a complex WT [2], [3]. More than 20 years ago, Grossman and Morlet [4] developed the continuous WT [5]. A revival of interest in later years has occurred in both signal processing and statistics for the use of complex wavelets [6], and complex analytic wavelets, particularly in [7]–[9]. It may be linked to the development of complex-valued discrete wavelet filters [10] and the clever dual filter bank [7], [5]. The complex WT has been shown to provide a powerful tool in signal and image analysis [11]. In [12], the authors derived large classes of wavelets generalizing the concept of the 1-D local complex-valued analytic decomposition introducing 2-D vector-valued hyperanalytic decompositions. In this paper, we propose the use of a very simple implementation of the hyperanalytic WT (HWT), recently proposed in [13]. Section II is about this new implementation. Section III is dedicated to image denoising. The paper concludes with a few final remarks.

Manuscript received January 9, 2008; revised September 18, 2008. The Associate Editor coordinating the review process for this paper was Dr. Annamaria Varkonyi-Koczy.

I. Firoiu is with the Communications Department, Electronics and Telecommunications Faculty, "Politehnica" University of Timisoara, 300223 Timisoara, Romania, and also with the Department of Signal and Communications, Telecom Bretagne, Institut Telecom, Centre National de la Recherche Scientifique, Université Européenne de Bretagne, 29238 Brest, France (e-mail: ioana.firoiu@etc.upt.ro).

C. Nafornita and A. Isar are with the Communications Department, Electronics and Telecommunications Faculty, "Politehnica" University of Timisoara, 300223 Timisoara, Romania (e-mail: corina.nafornita@etc.upt.ro; alexandru.isar@etc.upt.ro).

J.-M. Boucher is with the Department of Signal and Communications, Telecom Bretagne, Institut Telecom, Centre National de la Recherche Scientifique, Université Européenne de Bretagne, 29238 Brest, France (e-mail: jm.boucher@telecom-bretagne.eu).

Digital Object Identifier 10.1109/TIM.2009.2016382

II. New Implementation of the HWT

The shift sensitivity of the DWT is generated by the downsamplers used for its computation. In [11] and [14], the undecimated DWT (UDWT) is presented, which is a WT without downsamplers. Although the UDWT is shift insensitive, it has high redundancy 2^J (where J represents the number of iterations of the WT). In [15], a new shift-invariant but very redundant WT, named shift-invariant discrete WT, was proposed. It is based on an algorithm called cycle spinning, and it was conceived to suppress the artifacts in the neighborhood of discontinuities introduced by the DWT in denoising applications. For a range of delays, data are shifted, their DWT is computed, and then, the result is unshifted. Averaging the several obtained results, a quasi-shift-invariant DWT is implemented. In [16], it is demonstrated that approximate shiftability is possible for the DWT with a small fixed amount of transform redundancy. In this reference, a pair of real mother wavelets is designed such that one is approximately the Hilbert transform of the other. In the following, we will give the mathematical basis for this approach. In [17], the author provides a way to build new complete orthonormal sets of the Hilbert space of finite-energy band-limited functions with bandwidth π, named the Paley–Wiener (PW) space. He proved the following proposition.

P1. Let χ denote the characteristic function of the interval $[-\pi, \pi]$ and let $\mu(x)$ be real valued and piecewise continuous there. Then, the integer translations of the inverse Fourier transform of $\chi e^{i\mu}$ constitute a complete orthonormal set in PW.

Following this proposition, some new orthonormal complete sets of integer translations of a generating function can be constructed in the PW space. The scaling function and the mother wavelets of the standard multiresolution analysis of PW generate by integer shifts such complete orthonormal sets. Proposition P1 was generalized in [18] to give a new mechanism of mother wavelet construction. In this reference, the following two propositions were formulated.

P2. If $A_m = \{\alpha_{m,n}(t)\}|_{n\in Z}$ is a complete orthonormal set generating a Hilbert space H_m, then the set $\hat{A}_m = \{(1/2\pi)^{1/2} \cdot \alpha^{\wedge}_{m,n}(\omega)\}|_{n\in Z}$ is a complete orthonormal

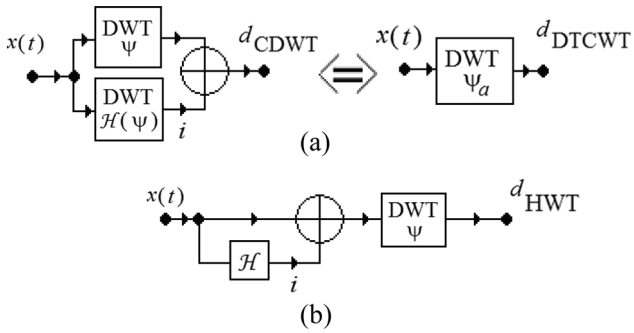

Fig. 1. Implementations of (a) the DTCWT and (b) the HWT are equivalent.

set of $\hat{H}_m$ (the Hilbert space composed by the Fourier transforms of the elements of the space H_m) and *vice versa*.

P3. If $\mu(\omega)$ is a real-valued and piecewise-continuous function and $\hat{A}_m = \{(1/2\pi)^{1/2} \cdot \alpha^{\wedge}_{m,n}(\omega)\}|_{n\in Z}$ is a complete orthonormal set of $\hat{H}_m$, then ${}_{\mu}\hat{A}_m = \{(1/2\pi)^{1/2} \exp(i\mu(\omega))\alpha^{\wedge}_{m,n}(\omega)\}|_{n\in Z}$ is another complete orthonormal set of the same space.

These two propositions can be used to build new mother wavelets if we identify the subspaces of an orthogonal decomposition of the Hilbert space $L^2(R)$, W_m, $m \in Z$, with the Hilbert spaces $\hat{H}_m$. With respect to this, the function $\mu(\omega)$ must satisfy the following constraint: $\mu(\omega) = \mu(2^m\omega), \forall m \in Z$.

An example of a function that satisfies this constraint is $\mu(\omega) = (\pi/2)(\mathrm{sgn}\omega + 1)$. In this case, $\exp(i\mu(\omega)) = \mathrm{sgn}(\omega)$. Therefore, the function generating the set ${}_{\mu}A_m$ (which corresponds to the new mother wavelets) is obtained by applying the Hilbert transform to the function generating the set A_m (which corresponds to the initial mother wavelets) multiplied by i. Consequently, if the function Ψ is a mother wavelet, then the functions $i\mathcal{H}\{\Psi\}$ and $\Psi_a = \Psi + i\mathcal{H}\{\Psi\}$ are also mother wavelets. This wavelet pair $(\Psi, i\mathcal{H}\{\Psi\})$ defines a complex DWT (CDWT), presented in Fig. 1(a). A complex wavelet coefficient is obtained by interpreting the wavelet coefficient from one DWT tree as being its real part, whereas the corresponding coefficient from the other tree is considered to form its imaginary part.

In [2], the double-tree complex WT (DTCWT), which is a quadrature pair of DWT trees similar to the CDWT, is developed. The DTCWT coefficients may be interpreted as arising from the DWT associated with a quasi-analytic wavelet. Both DTCWT and CDWT are invertible and quasi shift invariant.

The implementation of the HWT representing the aim of our proposal is presented in Fig. 1(b). First, we apply a Hilbert transform to the data. The real WT is then applied to the analytical signal associated to the input data, obtaining complex coefficients. The two implementations presented in Fig. 1 are equivalent because

$$\begin{aligned} d_{\mathrm{DTCWT}}[m,n] &= \langle x(t), \Psi_{m,n}(t) + i\mathcal{H}\{\Psi_{m,n}(t)\}\rangle \\ &= \langle x(t), \Psi_{m,n}(t)\rangle - i\langle x(t), \mathcal{H}\{\Psi_{m,n}(t)\}\rangle \\ &= \langle x(t), \Psi_{m,n}(t)\rangle + i\langle \mathcal{H}\{x(t)\}, \Psi_{m,n}(t)\rangle \\ &= \langle x(t) + i\mathcal{H}\{x(t)\}, \Psi_{m,n}(t)\rangle = d_{\mathrm{HWT}}[m,n]. \end{aligned} \quad (1)$$

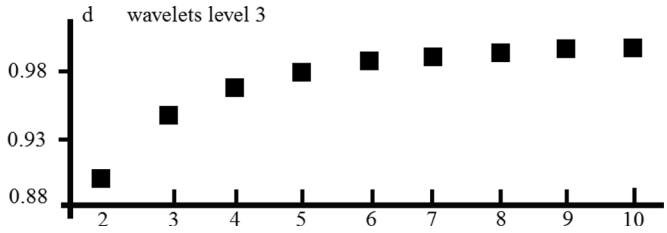

Fig. 2. Degree of shift invariance of HWT as a function of the regularity of the mother wavelet used for its computation.

Whereas the DTCWT requires special mother wavelets, the implementation of the HWT proposed in Fig. 1(b) can be done using classical mother wavelets like those introduced by Daubechies. These two transforms have a redundancy of two in the 1-D case. In [19], a two-stage mapping-based complex WT that consists of a mapping onto a complex function space followed by a DWT of the complex mapping computation is proposed. The authors observed that DTCWT coefficients may be interpreted as the coefficients of a DWT applied to a complex signal associated with the input signal. The complex signal is defined as the Hardy-space image of the input signal. As the Hardy-space mapping of a discrete signal cannot be computed, they defined a new function space called the Softy space, which is an approximation of the Hardy space. In [20], a new measure of the shift invariance is defined, called "shiftability." We introduced a new criterion: the degree of shift invariance d. It requires the computation of the values of the energy of every set of detail coefficients (at different decomposition levels) and of the approximation coefficients, corresponding to a certain delay (shift) of the input signal samples. This way, we obtain a sequence of energy values at each decomposition level, each sample of this sequence corresponding to a different shift. Then, using the mean m and the standard deviation sd of every energy sequence, the degree of shift invariance is

$$d = 1 - sd/m. \quad (2)$$

It can be increased if the absolute values of the wavelet coefficients are considered. In Fig. 2, the dependence of the degree of shift invariance of the new implementation is shown with respect to the regularity of the mother wavelets used for its computation, when the absolute values of the wavelet coefficients are considered.

The procedure followed in this simulation is described in [13]. The Daubechies family was investigated, each element being indexed by its number of vanishing moments. As the curve illustrated in Fig. 2 indicates, the degree of shift invariance increases with the degree of regularity of the mother wavelets used.

The generalization of the analyticity concept in 2-D is not obvious, as there are multiple definitions of the Hilbert transform in this case. In the following, we will use the definition leading to the so-called hypercomplex signal. The hypercomplex mother wavelet associated to $\Psi(x,y)$ is defined as

$$\begin{aligned} \Psi_a(x,y) = \Psi(x,y) &+ i\mathcal{H}x\{\Psi(x,y)\} \\ &+ j\mathcal{H}_y\{\Psi(x,y)\} + k\mathcal{H}_x\{\mathcal{H}_y\{\Psi(x,y)\}\} \end{aligned} \quad (3)$$

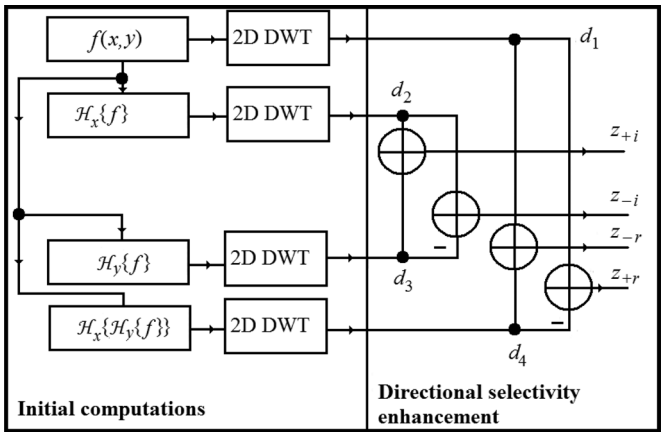

Fig. 3. New 2-D-HWT-implementation architecture.

where $i^2 = j^2 = -k^2 = -1$, and $ij = ji = k$ [21]. The HWT of the image $f(x, y)$ is

$$\mathrm{HWT}\{f(x,y)\} = \langle f(x,y), \Psi_a(x,y)\rangle\,. \tag{4}$$

Taking into account relation (3), it can be written as

$$\begin{aligned}\mathrm{HWT}\{f(x,y)\} &= \mathrm{DWT}\{f(x,y)\} + i\mathrm{DWT}\{\mathcal{H}_x\{f(x,y)\}\}\\ &\quad + j\mathrm{DWT}\{\mathcal{H}_y\{f(x,y)\}\}\\ &\quad + k\mathrm{DWT}\{\mathcal{H}_y\{\mathcal{H}_x\{f(x,y)\}\}\}\\ &= \langle f_a(x,y), \Psi(x,y)\rangle\\ &= \mathrm{DWT}\{f_a(x,y)\}\,.\end{aligned} \tag{5}$$

Therefore, the 2-D HWT of the image $f(x, y)$ can be computed with the aid of the 2-D DWT of its associated hypercomplex image. The new HWT implementation [13], [22], presented in Fig. 3, uses four trees, each one implementing a 2-D DWT. The first tree is applied to the input image. The second and the third trees are applied to 1-D discrete Hilbert transforms computed across the lines ($\mathcal{H}_x$) or columns ($\mathcal{H}_y$) of the input image. The fourth tree is applied to the result obtained after the computation of the two 1-D discrete Hilbert transforms of the input image. The enhancement of the directional selectivity of the 2-D HWT is made as in the case of the 2-D DTCWT [3], [5], by linear combinations of detail coefficients belonging to each subband of each of the four 2-D DWTs. This technique is explained, based on an example, in [22].

III. Image Denoising

During acquisition and transmission, images are often corrupted by additive noise. The aim of an image denoising algorithm is then to reduce the noise level, while preserving the image features. There is a big diversity of estimators used as denoising systems. One may classify these systems into two categories: those directly applied to the signal and those who use a WT before processing. In fact, Donoho and Johnstone introduced the word denoising in association with the wavelet theory [1]. From the first category, we must mention the denoising systems proposed in [23] and [24]. The first one is based on the shape-adaptive DCT that can be computed on a support of arbitrary shape. The second one is a maximum *a posteriori* (MAP) filter that acts in the spatial domain.

The multiresolution analysis performed by the WT has been shown to be a powerful tool to achieve good denoising. In the wavelet domain, the noise is uniformly spread throughout the coefficients, while most of the image information is concentrated in the few largest ones (sparsity of the wavelet representation) [25]–[33]. The corresponding denoising methods consist of three steps [1]: 1) the computation of the forward WT; 2) the filtering of the wavelet coefficients; and 3) the computation of the IWT of the result obtained. Consequently, there are two tools to be chosen: the WT and the filter. In what concerns the first choice, we propose in this paper the new implementation of the HWT. In [25] and [27], the UDWT was used; in [26], [28], and [31], the DTCWT was used; and in [29] and [30], the DWT was used. Concerning the second choice, numerous nonlinear filter types can be used in the WT domain. A possible classification is based on the nature of the noise-free component of the image to be processed. Basically, there are two categories of filters: those built assuming only the knowledge of noise statistics (a nonparametric approach) and those based on the knowledge of both signal and noise statistics (a parametric approach). From the first category, we can mention the hard-thresholding filter [1], the soft-thresholding filter (stf) [1], [11], which minimizes the min-max estimation error, and the efficient Stein's-unbiased-risk-estimate-based interscale pointwise thresholding filter [30], which minimizes the mean square error (MSE). To the second category belong filters obtained by minimizing a Bayesian risk under a cost function, typically a delta cost function (MAP estimation [25], [26], [28]) or the minimum MSE (minimum MSE estimation [27]). The denoising algorithms proposed in [26]–[30] exploit the interscale dependence of wavelet coefficients. The method proposed in [27] takes into account the intrascale dependence of wavelet coefficients as well. The statistical distribution of the wavelet coefficients changes from scale to scale. The coefficients for the first iterations of the WT have a heavy-tailed distribution. To deal with this mobility, there are two solutions. The first one assumes the use of a fixed simple model, risking a decrease of accuracy across the scales. This way, there is a chance to obtain a closed-form input–output relation for the MAP filter. Such an input–output relationship has two advantages: it simplifies the implementation of the filter, and it allows the sensitivity analysis. The second solution assumes the use of a generalized model, defining a family of distributions and the identification of the best fitting element of this family to the distribution of the wavelet coefficients at a given scale (e.g., the family of Pearson's distributions in [25], the family of $\mathrm{S}\alpha\mathrm{S}$ distributions in [28], and the model of Gauss–Markov random field in [29]). The use of a generalized model makes the treatment more accurate but requires implicit solutions for the MAP filter equation, which can often only numerically be solved. The MAP estimation of u, based on the observation $z = u + n$ (where n represents the WT of the noise, and u represents the WT of the useful component of the input image), is given by the MAP filter equation $\hat{u}(z) = \arg\max_u\{\ln(p_n(z-u)p_u(u))\}$, where p_a represents the probability density function (pdf) of a.

If the pdf's p_u and p_n do not take into account the interscale dependence of the wavelet coefficients, the obtained filter is called marginal. For the MAP filters that take into account the interscale dependence, the pdf's are multivariate functions. In the following, we consider a univariate Gaussian distribution for the noise coefficients (p_n) and a univariate Laplacian distribution for the useful signal coefficients (p_u). The noise coefficients have zero mean and variance σ_n^2.

A. Solution of the MAP Filter Equation

Consequently, we take

$$p_u(u) = \left(1/\left(2^{1/2}\sigma_u\right)\right) \exp\left(-2^{1/2}|u|/\sigma_u\right). \quad (6)$$

Under the considered hypothesis, the MAP filter equation becomes

$$(z-\hat{u})/\sigma_n^2 - \left(2^{1/2}/\sigma_u\right) \operatorname{sgn} \hat{u} = 0. \quad (7)$$

Finally, the solution corresponding to the proposed marginal MAP filter (pmMAPf) can be expressed as

$$\hat{u} = \operatorname{sgn}(z)\left(|z| - \left(2^{1/2}\sigma_n^2\right)/\sigma_u\right)_+ \quad (8)$$

where $(X)_+ = X$ for $X > 0$ and 0 otherwise. In (8), σ_n^2 is the noise variance, and σ_u is the standard deviation of the useful image coefficients. The relation (8) reduces to a soft thresholding of the noisy coefficients with a variable threshold. In the nonparametric approach, this threshold has a constant value, proportional to the noise standard deviation [1]. As an alternative, we use a denoising method based on the association of the DWT with an stf, where the already-mentioned constant of proportionality equals two, called adaptive stf. In practice, the statistical parameters in (8) are not known, and therefore, we use their estimates. To estimate σ_n^2 from the noisy wavelet coefficients, a robust median estimator is applied to the finest scale wavelet coefficients corresponding to each of the four DWTs

$$\hat{\sigma_n^2} = \text{median}\left(|z_i|\right)/0.6745, \qquad z_i \in \text{subband HH}. \quad (9)$$

The marginal variance of the kth coefficient is estimated using neighboring coefficients in the region $N(k)$, a window centered at the kth coefficient. To make this estimation, one gets $\sigma_z^2 = \sigma_u^2 + \sigma_n^2$, where σ_z^2 is the marginal variance of noisy observations y. For the estimation of σ_z^2, the following relationship is used:

$$\hat{\sigma}_z^2 = (1/M)\Sigma_{zi\in N(k)} z_i^2 \quad (10)$$

where M is the size of the neighborhood $N(k)$. Then, σ_u can be estimated as

$$\hat{\sigma}_u = \left(\hat{\sigma_z^2} - \hat{\sigma_n^2}\right)_+^{1/2}. \quad (11)$$

This estimation is not very accurate. In addition, after computing the sensitivities of that MAP filter with the noise and the clean image standard deviations [given in (9) and (11)], it can be observed that the absolute values of those sensitivities increase with the increase of $\hat{\sigma}_n$ and with the decrease of $\hat{\sigma}_u$, respectively. These behaviors must be counteracted. A solution is the use of a denoising algorithm in two stages [31].

B. Directional Windows in the Wavelet Domain

In [26], the regions $N(k)$ were rectangular of size 7×7. The energy clusters in different subbands are mainly distributed along the corresponding preferential directions. For this reason, the estimator using a squared window often leads to downward-biased estimates within and around energy clusters, which is disadvantageous for the preservation of edges and textures in images. In [31], the elliptic directional windows are introduced to estimate the signal variances in each oriented subband. We generalized here this idea for the proposed implementation of the 2-D-HWT associated with pmMAPf, using constant array elliptic estimation windows with their main axes oriented following the directions $\pm\text{atan}(1/2)$, $\pm\pi/4$, and $\pm\text{atan}(2)$.

C. Proposed Denoising Method

First stage: After applying the pmMAPf in the HWT domain, using elliptic estimation windows, a first partial result $\hat{u}_l^{\text{HWT}-\text{MAP}}$ is obtained. The local standard deviation of each pixel is computed into a rectangular window of size 7×7, obtaining an image $stdev$ that will lead the entire algorithm. To further enhance the denoising process, the image $stdev$ is used as follows. The maximum local standard deviation $stdev_{\max}$ is extracted and used to segment this image. Two classes are obtained, with elements separated by a threshold equal to 0.1 $stdev_{\max}$. These classes are used as masks. The second class, containing the higher values of the local standard deviations, is associated with the first partial result. Pixels, having the same coordinates as those belonging to the second class, are transferred into an intermediate result

$$inres_l(i,j) = \begin{cases} \hat{u}_l^{\text{HWT}-\text{MAP}}(i,j), & \text{if } stdev(i,j) > 0.1 stdev_{\max} \\ 0, & \text{otherwise} \end{cases}$$

where $l = 2, \ldots, 10$ vanishing moments.

Second stage: The adaptive stf is applied in the DWT domain for the same input image (using the same mother wavelets), obtaining a second partial result $\hat{u}_l^{\text{DWT}-\text{stf}}$. The intermediate result will be completed with the pixels of the second partial result having the same coordinates as those belonging to the first class of the $stdev$ image

$$inres_l(i,j) = \begin{cases} \hat{u}_l^{\text{HWT}-\text{MAP}}(i,j) & \text{if } stdev(i,j) > 0.1 stdev_{\max} \\ \hat{u}_l^{\text{DWT}-\text{stf}}(i,j) & \text{otherwise} \end{cases}$$

where $l = 2, \ldots, 10$ vanishing moments.

Third stage: A way to reduce the sensitivity of the denoising results with respect to the mother wavelet selection is the

TABLE I
COMPARISON OF THE CONTOUR TREATMENT OF THE PROPOSED DENOISING METHOD AND ITS COMPONENTS

σ_n	Noisy	l=8		HWT-pmMAPf	DWT-adaptive stf	Prop.
		Best par.	Best non-par			
10	3418	348	1018	615	1397	443
25	6458	921	1484	1544	2296	1373
35	7019	1360	1695	1882	2497	1806

TABLE II
COMPARISON OF THE HOMOGENEOUS-REGION TREATMENT OF THE PROPOSED DENOISING METHOD AND OF ITS COMPONENTS (R)

σ_n	Noisy	l=6		HWT-pmMAPf	DWT-adaptive stf	Prop.
		Best par.	Best non-par			
10	63	208	256	202	211	211
25	14	173	212	187	194	194
35	7	148	196	153	175	167

diversity enhancement. The first two stages are repeated for each of the nine mother wavelets from the family proposed by Daubechies (having a number of vanishing moments between two and ten), obtaining nine intermediate results. The final result is obtained by computing their mean

$$fires(i,j) = (1/9)\sum_{l=2}^{10} inres_1(i,j).$$

D. Simulation Results

In the following, some simulation results obtained using the image Lena (size 512 × 512) perturbed with additive white Gaussian noise are presented. Three types of results were considered. The association of the first and third stages

$$\hat{u}^{\mathrm{HWT-pmMAPf}}(i,j) = (1/9)\sum_{l=2}^{10} \hat{u}_l^{\mathrm{HWT-MAP}}(i,j)$$

is denoted by HWT–pmMAPf in Tables I–III. DWT–adaptive stf refers to the combination of the second and third stages

$$\hat{u}^{\mathrm{DWT-adaptive\ stf}}(i,j) = (1/9)\sum_{l=2}^{10} \hat{u}_l^{\mathrm{DWT-stf}}(i,j).$$

The complete denoising method based on the association of all of the three stages produces the *fires* and is named Prop. in the following.

We consider two types of simulations. The first one refers to the visual aspect of the image, while the latter focuses on the peak signal-to-noise ratio (PSNR) enhancement.

Generally, an image contains three types of regions: contours, textures, and homogeneous areas. We propose new measures of the contours and homogeneous region degradations due to denoising. First, the contours of the useful component of the input image and of the denoising results were detected, and the absolute values of the sums of contour approximation errors were computed. A small value of the sum indicates a good-quality treatment (the denoising preserves the contours). The results obtained are presented in Table I. The best results are obtained using the monowavelet parametric method (Best par.) when the mother wavelet Dau8($l = 8$) is used, followed by the results obtained using the method Prop. The quality of a homogeneous region denoising can be measured by computing the ratio of the square of its mean and its variance R. The corresponding simulation results can be found in Table II. The best method is the monowavelet nonparametric one (Best non-par.), when the mother wavelet Dau6 is used, very closely followed by the method named DWT–adaptive stf and the method Prop.

The second set of simulations is presented in Table III, and it refers to the PSNR enhancement. Let s and $\hat{s}$ be the noise-free (original) and the denoised images. The root mean square of the approximation error is given by $\varepsilon = ((1/N)\Sigma_q(s_q - \hat{s}_q)^2)^{1/2}$, where N is the number of pixels. The PSNR in decibels is $\mathrm{PSNR} = 20\log_{10}(255/\varepsilon)$. The best results are obtained using HWT–pmMAPf, which outperforms the results reported in [31] and [33], proving the efficiency of the proposed MAP system. These results are followed by the results of the method Prop. In fact, these results are comparable (slightly better) with the results obtained using another WT with enhanced directionality, i.e., the contourlet transform associated with a filtering method using directional estimation windows, reported in [32]. From the PSNR enhancement point of view, the denoising methods proposed in this paper are slightly inferior to the best results obtained in [26]–[28]. The images corresponding to $\sigma_n = 35$ are presented in Fig. 4. The visual aspects of the results obtained are satisfactory: the noise was completely eliminated, the contours are highlighted, and the homogeneous regions are uniform.

It is also interesting to evaluate the various denoising methods by the computation time. In this respect, the three proposed denoising methods are classified in the following order: DWT–adaptive stf, HWT–pmMAPf, and Prop.

IV. CONCLUSION

The HWT is a very modern WT as it has been formalized only two years ago [12]. In this paper, we have used a simple implementation of this transform, which permits the exploitation of the mathematical results and of the algorithms previously obtained in the evolution of wavelet theory. This implementation has a very flexible structure, as we can use any orthogonal or biorthogonal real mother wavelets for the computation of the HWT. We have preferred a denoising strategy based on diversity enhancement, on a simple MAP filter and on the estimation of the local standard deviation using directional windows. The simulation results in Table III illustrates the effectiveness of the proposed association HWT–pmMAPf.

To appreciate the contribution of the new implementation of the HWT and of the proposed MAP filter, Table III compares the method HWT–pmMAPf with the denoising association DWT–Wiener filter based on the genuine use of directional estimation windows [31]. Our results are slightly better.

Two new ideas have been proposed in this paper. The first one refers to the diversity enhancement. Its useful effect is the increase of 0.6 dB of the output PSNR of Prop. with respect

TABLE III
COMPARISON OF THE PSNRS OBTAINED USING DIFFERENT DENOISING METHODS REPORTED IN THE REFERENCES INDICATED (IN DECIBELS)

σ_n	Noisy	[31]	[32]	[33]	l=10		HWT-pmMAPf	DWT- adaptive stf	Prop.
					Best par.	Best non-par.			
10	28.18	*34.7*	-	-	34.06	31.6	**34.92**	31.4	34.54
20	22.16	*31.5*	-	31.58	-	-	**31.6**	28.56	31.42
25	20.20	*30.4*	-	-	29.67	27.85	**30.55**	27.63	30.37
30	18.62	-	28.77	-	-	-	**29.61**	26.91	*29.45*
35	17.29	-	-	-	28.01	26.44	**28.83**	26.28	*28.65*
40	16.53	-	27.47	27.74	-	-	**28.13**	25.75	*27.93*
50	14.18	-	26.46	-	-	-	**26.96**	24.84	*26.63*

Fig. 4. Top: Noisy image. Bottom: Denoising result (Prop.).

to the best monowavelet intermediate result. The drawback of the diversity enhancement is a slight degradation of the visual aspect quality. The second new idea proposed is the cooperation between a parametric and a nonparametric denoising technique. Despite the small output PSNR reduction, the hybrid approach (Prop.) enhances the visual aspect of the HWT–pmMAPf.

A future research direction will be the speed optimization of our codes. Another research direction will be the segmentation threshold selection optimization (the value 0.1 $stdev$ has been empirically chosen). Finally, we will find better solutions for the intermediate-result synthesis.

The comparisons made in this paper suggest that the new image denoising results are competitive with some of the best wavelet-based results reported in the literature, despite the inaccuracy of the statistical model used.

ACKNOWLEDGMENT

The authors would like to thank the anonymous reviewers for the very competent and efficient aid they have given.

REFERENCES

[1] D. L. Donoho and I. M. Johnstone, "Ideal spatial adaptation by wavelet shrinkage," *Biometrika*, vol. 81, no. 3, pp. 425–455, 1994.
[2] N. Kingsbury, "Complex wavelets for shift invariant analysis and filtering of signals," *Appl. Comput. Harmon. Anal.*, vol. 10, no. 3, pp. 234–253, May 2001.
[3] N. G. Kingsbury, "A dual-tree complex wavelet transform with improved orthogonality and symmetry properties," in *Proc. IEEE Conf. Image Process.*, Vancouver, BC, Canada, Sep. 2000, pp. 375–378.
[4] A. Grossman and J. Morlet, "Decomposition of hardy functions into square integrable wavelets of constant shape," *SIAM J. Math. Anal.*, vol. 15, no. 4, pp. 723–736, Jul. 1984.
[5] I. W. Selesnick, R. G. Baraniuk, and N. G. Kingsbury, "The dual-tree complex wavelet transform," *IEEE Signal Process. Mag.*, vol. 22, no. 6, pp. 123–151, Nov. 2005.
[6] S. Barber and G. P. Nason, "Real nonparametric regression using complex wavelets," *J. Roy. Stat. Soc. B*, vol. 66, no. 4, pp. 927–939, Nov. 2004.
[7] N. G. Kingsbury, "Image processing with complex wavelets," *Philos. Trans. Roy. Soc. London A, Math. Phys. Sci.*, vol. 357, pp. 2543–2560, 1999.
[8] I. W. Selesnick, "The design of approximate Hilbert transform pairs of wavelet bases," *IEEE Trans. Signal Process.*, vol. 50, no. 5, pp. 1144– 1152, May 2002.
[9] I. W. Selesnick, "Hilbert transform pairs of wavelet bases," *IEEE Signal Process. Lett.*, vol. 8, no. 6, pp. 170–173, Jun. 2001.
[10] J.-M. Lina and M. Mayrand, "Complex Daubechies wavelets," *Appl. Comput. Harmon. Anal.*, vol. 2, no. 3, pp. 219–229, Jul. 1995.
[11] S. Mallat, *A Wavelet Tour of Signal Processing*, 2nd ed. New York: Academic, 1999.
[12] S. C. Olhede and G. Metikas, "The hyperanalytic wavelet transform," Dept. Math., Imperial College, London, U.K., Imperial College Statistics Section Tech. Rep. TR-06-02, May 2006.
[13] I. Adam, C. Nafornita, J.-M. Boucher, and A. Isar, "A new implementation of the hyperanalytic wavelet transform," in *Proc. IEEE ISSCS*, Iasi, Romania, 2007, pp. 401–404.
[14] M. Lang, H. Guo, J. E. Odegard, C. S. Burrus, and R. O. Wells, Jr., "Noise reduction using an undecimated discrete wavelet transform," *IEEE Signal Process. Lett.*, vol. 3, no. 1, pp. 10–12, Jan. 1996.
[15] R. Coifman and D. Donoho, "Translation invariant de-noising," in *Wavelets and Statistics*, A. Antoniadis and G. Oppenheim, Eds. New York: Springer-Verlag, 1995, pp. 125–150.
[16] P. Abry, "Transformées en ondelettes-Analyses multirésolution et signaux de pression en turbulence," Ph.D. dissertation, Université Claude Bernard, Lyon, France, 1994.
[17] J. R. Higgins, "Bases for the Hilbert space of Paley-Wiener functions," in *Proc. Aachener Colloq.*, 1984, pp. 274–278.

[18] A. Isar, *Nouvelles modalités de décomposition multiresolution des signaux à energie finie*. Juan-les-Pins, France: Quatorzieme Colloque GRETSI, 1993, pp. 93–97.
[19] F. C. A. Fernandes, R. L. C. van Spaendonck, and C. S. Burrus, "A new framework for complex wavelet transforms," *IEEE Trans. Signal. Process.*, vol. 51, no. 7, pp. 1825–1837, Jul. 2003.
[20] E. P. Simoncelli, W. T. Freeman, E. H. Adelson, and D. J. Heeger, "Shiftable multi-scale transforms," *IEEE Trans. Inf. Theory*, vol. 38, no. 2, pp. 587–607, Mar. 1992.
[21] C. Davenport, *Commutative Hypercomplex Mathematics*. [Online]. Available: http://home.usit.net/~cmdaven/cmdaven1.htm
[22] I. Adam, C. Nafornita, J.-M. Boucher, and A. Isar, "A Bayesian approach of hyperanalytic wavelet transform based denoising," in *Proc. IEEE Int. Conf. WISP*, Alcala de Henares, Spain, Oct. 2007, pp. 237–242.
[23] A. Foi, V. Katkovnik, and K. Egiazarian, "Pointwise shape-adaptive DCT for high-quality denoising and deblocking of grayscale and color images," *IEEE Trans. Image Process.*, vol. 16, no. 5, pp. 1395–1411, May 2007.
[24] M. Walessa and M. Datcu, "Model-based despeckling and information extraction from SAR images," *IEEE Trans. Geosci. Remote Sens.*, vol. 38, no. 5, pp. 2258–2269, Sep. 2000.
[25] S. Foucher, G. B. Benie, and J.-M. Boucher, "Multiscale MAP filtering of SAR images," *IEEE Trans. Image Process.*, vol. 10, no. 1, pp. 49–60, Jan. 2001.
[26] L. Sendur and I. W. Selesnick, "Bivariate shrinkage functions for wavelet-based denoising exploiting interscale dependency," *IEEE Trans. Signal Process.*, vol. 50, no. 11, pp. 2744–2756, Nov. 2002.
[27] A. Pizurica and W. Philips, "Estimating the probability of the presence of a signal of interest in multiresolution single and multiband image denoising," *IEEE Trans. Image Process.*, vol. 15, no. 3, pp. 654–665, Mar. 2006.
[28] A. Achim and E. E. Kuruoglu, "Image denoising using bivariate α-stable distributions in the complex wavelet domain," *IEEE Signal Process. Lett.*, vol. 12, no. 1, pp. 17–20, Jan. 2005.
[29] D. Gleich and M. Datcu, "Gauss-Markov model for wavelet-based SAR image despeckling," *IEEE Signal Process. Lett.*, vol. 13, no. 6, pp. 365–368, Jun. 2006.
[30] F. Luisier, T. Blu, and M. Unser, "A new SURE approach to image denoising: Inter-scale orthonormal wavelet thresholding," *IEEE Trans. Image Process.*, vol. 16, no. 3, pp. 593–606, Mar. 2007.
[31] P.-L. Shui, "Image denoising algorithm via doubly local Wiener filtering with directional windows in wavelet domain," *IEEE Signal Process. Lett.*, vol. 12, no. 10, pp. 681–684, Oct. 2005.
[32] Z.-F. Zhou and P.-L. Shui, "Contourlet-based image denoising algorithm using directional windows," *Electron. Lett.*, vol. 43, no. 2, pp. 92–93, Jan. 2007.
[33] S. C. Olhede, "Hyperanalytic denoising," Dept. Math., Imperial College, London, U.K., Imperial College Statistics Section Tech. Rep. TR-06-01 1.

Ioana (Adam) A. Firoiu was born in Deva, Romania, in 1982. She received the B.Sc. degree in electronic and telecommunications engineering in 2005. She is currently working toward the Ph.D. degree both in the Communications Department, Electronics and Telecommunications Faculty, "Politehnica" University of Timisoara, Timisoara, Romania, and in the Department of Signal and Communications, Telecom Bretagne, Institut Telecom, Centre National de la Recherche Scientifique, Université Européenne de Bretagne, Brest, France.

Her research interests include signal and image processing, multiresolution analysis, and wavelet theory.

Corina Nafornita (M'XX) was born in Timisoara, Romania. She received the B.E. and M.Sc. degrees in electrical engineering from the "Politehnica" University of Timisoara, Timisoara, Romania, in 2003 and 2004, respectively, and the Ph.D. degree in electrical engineering from the Technical University of Cluj-Napoca, Cluj-Napoca, Romania, in 2008.

In 2003, she joined the Communications Department, Electronics and Telecommunications Faculty, "Politehnica" University of Timisoara, where she is currently a Member of the Signal Processing Group and an Assistant Professor. She is a Reviewer for the *EURASIP Journal on Information Security*, *IET Information Security*, *Research Letters in Electronics*, *Journal of Systems and Software*, and *Signal Processing*. Her research interests include signal and image processing, multimedia security, watermarking, and wavelets.

Dr. Nafornita is a Reviewer for the IEEE TRANSACTIONS ON INFORMATION FORENSICS AND SECURITY and IEEE TRANSACTIONS ON MULTIMEDIA.

Jean-Marc Boucher (SM'XX) was born in 1952. He received the Engineering degree in telecommunications from the Ecole Nationale Supérieure des Telecommunications, Paris, France, in 1975 and the Habilitation à Diriger des Recherches degree from the University of Rennes 1, Rennes, France, in 1995.

He is currently a Professor with the Department of Signal and Communications, Telecom Bretagne, Institut Telecom, Centre National de la Recherche Scientifique (CNRS), Université Européenne de Bretagne, Brest, France, where he is also the Education Deputy Manager and the Deputy Head of the UMR CNRS 3192 lab-STICC research unit. He is the author of about 100 technical articles in international journals and conference proceedings. His current research interests include statistical signal analysis including estimation theory, Markov models, blind deconvolution, wavelets, and multiscale image analysis. These methods are applied to radar and sonar images, seismic signals, and electrocardiographic signals.

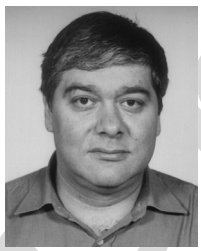

Alexandru Isar (M'XX) was born in 1957. He received the Engineering degree in electronics and telecommunication and the Ph.D. degree from the "Politehnica" University of Timisoara, Timisoara, Romania, in 1982 and 1993, respectively.

He is currently a Professor with the Communications Department, Electronics and Telecommunications Faculty, "Politehnica" University of Timisoara. He is the author of about 16 technical articles in international journals and conference proceedings. He is a Reviewer for the *Journal of Electronic Imaging* and *Signal Processing*. His current research interests include wavelets and signal and image processing. These methods are applied to sonar images and communication signals.

Dr. Isar is a Reviewer for the IEEE TRANSACTIONS ON INSTRUMENTATION AND MEASUREMENTS.

AUTHOR QUERIES

AUTHOR PLEASE ANSWER ALL QUERIES

AQ1 = Note that "reciprocally" was changed to "*vice versa*." Please check if appropriate.
AQ2 = Please specify the institution from which the author received the degree.
AQ3 = Note that "GET, ENST Bretagne, CNRS" was changed to "Telecom Bretagne, Institut Telecom, CNRS, Université Européenne de Bretagne" to match the information in the affnote. Please check if appropriate.
AQ4 = Please provide IEEE membership history.
AQ5 = Please provide IEEE membership history.
AQ6 = Note that "Ecole Nationale Superieure des Telecommunications de Bretagne" was changed to "Telecom Bretagne, Institut Telecom, Centre National de la Recherche Scientifique (CNRS), Université Européenne de Bretagne" to match the information in the affnote. Please check if appropriate.
AQ7 = Please provide IEEE membership history.

NOTE: Please check if Ref. [12] and [33] were captured correctly.

END OF ALL QUERIES